Cooling of a Late-Syn Orogenic pluton: Evidence from Laser K-feldspar Modelling of the Carion Granite, Madagascar

Joseph G. Meert[1,2], Chris Hall[3], Anne Nédélec[4] and Marie Madison-Razanatseheno[5]

[1]Norwegian Geological Survey, Geodynamics Group, Leiv Eirikssons vei 39, 7491 Trondheim, Norway

[2]Indiana State University, Department of Earth Sciences, Paleomagnetics Laboratory, Terre Haute, IN 47809

[3]University of Michigan, Department of Geological Sciences, 2534 CC Little Building, Ann Arbor, MI 48109

[4]Uiversité Paul Sabatier, UMR 5563 CNRS, 38 rue des 36-ponts, 31400 Toulouse, France

[5]Université d'Antananarivo, Faculté es Sciences, BP 906, Départment des Sciences de la Terre, Antananarivo, Madagascar

Gondwana Research

Dec 2000

Abstract

Since the late 1980's, it has been hypothesized that the wide range of apparent argon ages seen within single K-feldspar samples might be due to a distribution of diffusion domain sizes within the mineral. To test and apply this idea, an analytical technique which combines conventional laboratory degassing experiments (resistance heating) with numerical inversion procedures has been developed to extract cooling history information from feldspars. A key part of the method involves careful control of temperature in the laboratory to constrain the diffusion parameters of the feldspar samples. In our study, we have K-feldspar data from single crystals that mimic the types of data seen in classic resistance heater fusion experiments. Our step-heating data are based on using a continuous argon-ion laser with no direct control on temperature. However, with only a single added free parameter in the model, we show that it is possible to analyze this data in the multi-domain style, and make some simple inferences on the nature of the cooling history of the Carion pluton in central Madagascar. The Carion granitic pluton in central Madagascar was intruded into warm continental crust following orogenic events related to the final amalgamation of Gondwana. U-Pb SHRIMP dating of the pluton yields an emplacement age of 532.1 ± 2.1 Ma followed by relatively slow cooling as constrained by $^{40}Ar/^{39}Ar$ ages on hornblende, biotite and K-spar. Four hornblende samples yielded a mean $^{40}Ar/^{39}Ar$ age of 512.7 ± 1.3 Ma. A biotite sample yielded an age of 478.9 ± 1.0 Ma and modeled K-spar ages show cooling from 350° C at 466 Ma to 100° C by 410 Ma. Collectively, the data suggest that the pluton cooled from 850° C at 532.1 ± 5 (U-Pb zircon) Ma to 500° C at 512.7 ± 1.3 Ma ($^{40}Ar/^{39}Ar$ hornblende), or approximately 18 °C/Ma slowing to ~4 °C/Ma between 512 Ma and 478 Ma and finally to about 3°C/Ma between 478 and 410 Ma.

Key words: $^{40}Ar/^{39}Ar$ dating, Laser fusion, Gondwana, Madagascar, cooling history

1. Introduction

The island of Madagascar is located in a key position within the assembled Gondwana supercontinent (Figure 1). Geochronologic work in the past decade has provided important constraints on the evolution of the island (Paquette et al., 1994; Kröner et al., 1996; Ito et al., 1997; Paquette and Nedelec, 1998; Handke et al., 1999; Tucker et al., 1999a,b; Kröner et al., 2000). An excellent summary of these data is provided by Kröner et al. (2000).

Widespread magmatic activity in central Madagascar (granitoid and gabbroic intrusions) is dated between 824-740 Ma (Handke et al., 1999; Tucker et al., 1999a,b; Kröner et al., 2000). Handke et al. (1999) concluded that the magmatism resulted from Andean-type subduction beneath central Madagascar. Paquette and Nedelec (1998) dated 'stratoid' granites in central Madagascar. They reported U-Pb zircon ages of 627-633 Ma and interpreted the emplacement of these rocks in a post-collision extensional tectonic setting (Nedelec et al., 1995, 2000). A 611.7 ± 1.7 Ma $^{40}Ar/^{39}Ar$ plateau age on biotite (in progress by the author) supports these ages. According to Paquette and Nedelec (1998), Madagascar collided with East Africa at about 650 Ma and underwent extensional collapse at roughly 630 Ma.

The island of Madagascar experienced widespread thermal overprinting during the 500-570 Ma interval (see Kröner et al., 2000 and references therein). Meert (1999) attributed these ages to a younger collision between Australo-Antarctica and Madagascar. Kröner et al. (2000) argued that the granulite facies metamorphism in central Madagascar formed during extensional collapse as did Collins et al. (2000), but the locations of age determinations delineating this 'collapse' are closely associated with major shear zones. In southern Madagascar (south of the Bongolava-Ranotsara shear zone), Paquette et al. (1995) report granulite metamorphic ages between 523 and 577 Ma. These ages were used to argue for a high-grade regional metamorphic event between 565-580 Ma with the younger ages representing a thermal fluid disturbance in the isotopic systematics following high-grade regional metamorphism. Similar ages were obtained for the southern Madagascar domains by Andriamarofahatra et al. (1990), Nicollet et al. (1997) and Montel et al. (1994, 1996).

2. Geological setting & Previous Geochronology

The Carion granitic massif is situated to the east of Antananarivo. It is ~20 km in diameter and its elliptical shape is deeply indented in the north-west (Fig. 2). The Carion massif was emplaced near the western border of the Angavo shear belt (Fig. 2a), a major Panafrican structure that

parallels the eastern coast of Madagascar (Windley et al., 1994). Near Antananarivo, the Angavo belt is characterized by north-south steep foliations and shallowly plunging lineations acquired in low-pressure granulitic conditions (Ralison et al., 1997; Ralison, 1998; Nédélec et al., 2000). Paquette & Nédélec (1998) proposed that this shear zone was active from 570-550 Ma as were other major N-S shear zones in southern Madagascar (Paquette et al., 1994; Kröner et al., 1996).

Lautel (1953) first noted the post-tectonic setting of the Carion granite. The porphyritic nature of the rocks helps define steeply dipping magmatic lineations/foliations. In fact, the steep lineations contrast sharply with gently dipping lineations of the nearby Angavo shear belt (Nédélec et al., 2000; Meert et al., 2001). Incipient high-temperature solid-state deformation features (elongate quartz grains with occasional chessboard subgrain patterns) are observed in thin sections, but no orthogneissification is observed. Foliations in the country rocks are parallel with the massif, except in the northern indentation, where they are crosscut by the intrusion. The Carion massif shows no contact metamorphism at its margins. All of these data support a post-tectonic setting, but also show that the time lag between the formation of the Angavo shear belt (and its associated granulitic metamorphism) and the emplacement of the Carion magmas was short. Therefore both Nédélec et al. (2000) and Meert et al. (2001) assigned a late-syn tectonic setting for the Carion pluton.

The first attempt to date the Carion pluton by Vachette & Hottin (1974) resulted in two Rb/Sr isochron ages of 682 Ma and 527 Ma. The older age is likely devoid of any geological significance, as it was calculated using non-cogenetic rocks along with the typical Carion porphyritic granite. Kröner et al. (1999) reported a U-Pb evaporation age of 556 ± 1.7 Ma for the Carion pluton, but the location of the sample placed it outside the archetypal Carion massif. Indeed, we suggested that the 556 ± 1.7 Ma age (Kroner et al., 1999) dates the timing granulite formation in the nearby Angavo shear belt rather than the emplacement age of the Carion pluton (Meert et al., 2001). Subsequent dating of the pluton by Kröner et al. (2000) yielded a Pb-Pb age of 537.6 ± 1.0 Ma. Meert et al. (2001) used SHRIMP U-Pb methods and obtained a concordant age of 532.1 ± 5.1 Ma that overlaps with the age obtained by Kröner et al. (2001). $^{40}Ar/^{39}Ar$ dating of hornblende and bitoite from the Carion pluton by Meert et al. (2001) yielded ages of 512.7 ± 1.3 Ma and 478.9 ± 1.0 Ma respectively. Estimates of the closure temperatures for the minerals were also given in that study. The closure temperature estimates were 850° ± 50° C (U-Pb zircon), 500° ± 50° C for hornblende ($^{40}Ar/^{39}Ar$) and 350° ± 50° C for biotite ($^{40}Ar/^{39}Ar$).

3. Geochemistry/Emplacement Conditions

The main petrographic type of the Carion massif is a dark grey porphyritic granitoid of intermediate composition that can be easily identified in the field. The pluton displays a rough normal zoning ranging from tonalitic compositions at the rim to granodioritic and, locally, monzogranitic, compositions at the centre. Most rocks are porphyritic and contain conspicuous feldspar megacrysts with an average length of 2.5 cm. These megacrysts are generally perthitic orthoclase or microcline; in the more mafic rocks, they can also be plagioclase. Feldspars, both as megacrysts and as interstitial grains, constitute half the volume of the rocks. Plagioclase is generally unzoned and restricted to compositions in the range An_{24}-An_{26}, but can be as low as An_{10} in the most differentiated granite. Quartz is always present. Ferro-magnesian minerals amount to 10-25% of the modal compositions. They are mainly edenitic hornblende and biotite, both with xMg = 0.6-0.7. Relict orthopyroxene is observed in a few samples. Accessory minerals are present in noticeable amounts. Magnetite, apatite and zicon are ubiquitous, whereas titanite characterizes the most evolved rocks.

Representative major and trace element analyses are given in table 1 (reproduced from Madison-Razanatseheno, 1998). SiO_2 contents range from 61.62% to 73.49%. Actually, intermediate compositions predominate and the highest value corresponds to late magmatic veins in the center of the massif. In the diagram A/NK vs A/CNK of Fig. 3a, the rocks are metaluminous following the classification of Shand (1947) or I-type after Chappell & White (1974). In the K_2O vs SiO_2 diagram (Fig. 3b), they plot in the field of the high-K calc-alkaline series after Le Maître et al. (1989) or in the field of the shoshonitic series after Rickwood (1989). This is consistent with the noticeable abundance of K-feldspar (and hence of K_2O), even in the less evolved compositions. According to Liégeois et al. (1998), the low Na_20 contents at around 3% counterbalancing the high K_2O contents point to a shoshonitic trend rather than to a high-K calc-alkaline one. The Carion massif has a distinct ferriferous nature as can be seen from the Mg/Mg + Fe vs B diagram of Fig. 3c.

Among the trace elements, Ba appears especially abundant (1000-2300 ppm), but behaves as a compatible element controlled by the abundance of K-spar. Sr and Rb contents also display quite high values. Zr and Ce contents (respectively 388-762 and 176-327 ppm) are much higher than in typical I-type rocks, in agreement with the shoshonitic nature of the Carion massif. These high field-strength elements are hosted by accessory minerals and their abundance likely points to the

high-temperature character of the Carion magmas. In the Rb vs (Y + Nb) discrimination diagram of Pearce et al. (1984), the rocks plot in the field of within-plate granitoids (Fig. 3d)

Although geochemical data alone should not be used to identify the tectonic setting of the rocks because the geochemistry of magmatic rocks is likely to be influenced by the source (Chappell & Stephens, 1988), we note that the geochemistry of the Carion massif is consistent with its late- to post-tectonic setting. Indeed, high-K calc-alkaline or shoshonitic magmatism occurred also late in the Hercynian orogen of western Europe (Pagel & Leterrier, 1980; Debon & Lemmet, 1989), as well as in the Himalayan orogen of Tibet (Miller et al., 1999).

Emplacement conditions

Taking into account the late- to post-tectonic setting, the pressure calculations presented by Nédélec et al. (2000) are good estimates to infer the depth of emplacement of the Carion massif. Using the Al-in-hornblende barometer of Anderson & Smith (1995), these authors obtained a value of 3.3 (± 0.3) kb from a sample located 20 kilometers east of Carion and a value of 3.2 (± 0.1) kb from a sample located in the peripheral part of the Carion massif. Therefore, it is concluded that the Carion massif was emplaced at a depth of around 10-11 kilometers corresponding to these pressure conditions.

4. $^{40}Ar/^{39}Ar$ laser dating of K-spar

All argon age analyses were performed using a VG1200S mass spectrometer equipped with a Daly detector operated in analog mode. Samples were step-heated using a Coherent INNOVA model 70 argon ion laser with a nominal maximum output power of 5W. All analyses were performed with a fully automated fusion system, with laser power being set under computer control. Step-heating durations were 60 seconds, and the total fusion plus gas clean-up time was 3 minutes. Laser fusion system blanks were monitored frequently (typically every 5-6 fractions) and were normally about $1x10^{-13}$, $3x10^{-13}$, $3x10^{-14}$, $3x10^{-14}$, and $5x10^{-12}$ mlSTP for masses 36 through 40 respectively. The irradiation standard used was hornblende MMHb-1 with an assumed K-Ar age of 520.4 Ma (Samson and Alexander, 1987). Each irradiation consisted of a set of samples and standards sealed within evacuated fused silica tubes, and from each tube, at least 3 analyses for each of 5 packets

of MMHb-1 were analyzed. The resulting values of *J* were interpolated for each unknown sample location. Error estimates for *J* include scatter about the interpolation function. Mass discrimination in the mass spectrometer was monitored daily by analyzing an aliquot of atmospheric argon with a volume of about $5x10^{-9}$ mlSTP. Results are summarized in Table 2. Sample CAR-31 was taken from the center of the pluton (see Figure 2). Samples used in the previous study are also shown in Figure 2.

Since the late 1980's, it has been hypothesized that the wide range of apparent argon ages seen within single K-feldspar samples might be due to a distribution of diffusion domain sizes within the mineral. To test and apply this idea, an analytical technique which combines laboratory degassing experiments with numerical inversion procedures has been developed to extract cooling history information from feldspars (e.g. Lovera et al., 1989; Lovera et al., 1991). A key part of the method involves careful control of temperature in the laboratory to constrain the diffusion parameters of the feldspar samples. In our study, we have K-feldspar data from single crystals that mimic the types of data seen in classic resistance heater fusion experiments. Unfortunately, our step-heating data are based on using a continuous argon-ion laser with no direct control on temperature. However, with only a single added free parameter in the model, it may be possible to analyze this data in the multi-domain style, and make some simple inferences on the nature of the cooling history for the Carion granite.

The basic assumption to convert laser power into a proxy for temperature involves the mechanism for heat loss for a sample which is being laser step-heated. Hall et al. (1988) demonstrated, using data from an infra-red pyrometer, that to a very good approximation, cooling of a heated mineral grain in a UHV vacuum system could be accounted for simply via black-body radiation, and that thermal losses from conduction were negligible. Given this assumption, sample

temperature at steady state will be determined by a balance of laser power absorption and black-body radiation. Therefore, using the Stefan-Boltzmann law, the relationship between laser power and temperature can be written as:

$$aP = T^4 - T_0^4 \quad (1)$$

where P is laser power, T is absolute temperature, and T_0 is ambient temperature. The parameter α is a proportionality constant that will depend on the sample's reflectivity, emissivity, grain size, opacity, the laser beam size and other details of the system's optics. It is not possible to assign α accurately from first principles, but given the expected degassing temperatures for K-feldspars (400°-1100° C) and the actual laser powers used, we can roughly estimate that, for our experiments, α should have values of about 2 - 3 $x10^9$ with P measured in mW and T in Kelvin.

To model the ^{39}Ar release pattern, we used a modified version of the algorithm described in Hall (1990). In this method, the cumulative argon release pattern is fitted directly in the least squares sense, using a discrete suite of allowed domains. The problem is constrained by the fact that the contribution of each domain must be non-negative, and the total of all contributions must add up to one. This is a standard problem in quadratic programming and the specific algorithm used was adapted from Mifflin (1978). The suite of possible domains was a uniformly distributed set of 251 discrete domains having blocking temperatures (Dodson, 1973) ranging from 100° C to 350° C, using infinite slab geometry and assuming a cooling rate at blocking of 3 °C/Ma. Therefore, the allowed domain set had a temperature resolution of 1°C, which should be adequate for describing any reasonable set of actual domains. Using this method with resistance heater data, it can be shown that a broad range of diffusion activation energies can be made to fit laboratory data, as was argued by York and Hall (1990). Given that, plus the fact that we do not have direct laboratory temperature estimates, it was felt that it would not be possible to estimate this parameter from

our data and instead, a typical value for K-feldspar of 50 kcal/mol was assumed. That value, plus the constant α were the two free parameters in the fit of ^{39}Ar release. The maximum blocking temperature of 350° C was constrained by the fact that the K-feldspar ages are lower than the co-existing biotite ages, and 350° C is a reasonable blocking temperature estimate for our biotite as described by Meert et al. (2001).

Once the argon release pattern had been fit, the resulting set of domains with non-zero volume contributions were assigned argon blocking ages in order to fit the measured apparent age spectra. This was done assuming monotonic cooling from temperatures above the maximum allowed blocking temperature, and allowance was made for possible disturbances of each domain's age spectrum because of slow cooling through the blocking temperature. This correction used a method similar to that outlined in Onstott et al. (1989) and York (1984). The resulting age-temperature pairs can then be used as the basis for constructing a possible cooling history for the sample. Of course, the derived cooling trajectory is not the only possible cooling history that can fit the data; multiple episodes of reheating and argon loss are also possible. However, the fitted cooling trajectory will be close to the lowest possible cooling rates that can fit the data.

The K-feldspar data and the model fits to the age spectra (both ages and ^{39}Ar release) are shown in Figs. 4a-d. For both analyses, we show a range of models assuming a variety of α values. As can be seen from figures 4c,d , there the entire range of likely α values can give a very good fit to the data. The blocking age and blocking temperature pairs for the model domains are plotted in figures 5a,b. For both samples, the models show a cooling from about 350° C to about 200° C by about 430-440 Ma, with cooling to about 100° C by roughly 410 Ma. In figure 5c we show a possible composite series of blocking ages, with an α value for both samples of $2.8x10^9$. As can be seen from figure 5c, the models are broadly compatible with a cooling trend from 350° C at 480 Ma at a rate

Cooling of a Late-Syn Orogenic pluton: Evidence from Laser K-feldspar Modelling of the Carion Granite, Madagascar

Joseph G. Meert[1,2], Chris Hall[3], Anne Nédélec[4] and Marie Madison-Razanatseheno[5]

[1]Norwegian Geological Survey, Geodynamics Group, Leiv Eirikssons vei 39, 7491 Trondheim, Norway

[2]Indiana State University, Department of Earth Sciences, Paleomagnetics Laboratory, Terre Haute, IN 47809

[3]University of Michigan, Department of Geological Sciences, 2534 CC Little Building, Ann Arbor, MI 48109

[4]Uiversité Paul Sabatier, UMR 5563 CNRS, 38 rue des 36-ponts, 31400 Toulouse, France

[5]Université d'Antananarivo, Faculté es Sciences, BP 906, Départment des Sciences de la Terre, Antananarivo, Madagascar

Gondwana Research

Dec 2000

Abstract

Since the late 1980's, it has been hypothesized that the wide range of apparent argon ages seen within single K-feldspar samples might be due to a distribution of diffusion domain sizes within the mineral. To test and apply this idea, an analytical technique which combines conventional laboratory degassing experiments (resistance heating) with numerical inversion procedures has been developed to extract cooling history information from feldspars. A key part of the method involves careful control of temperature in the laboratory to constrain the diffusion parameters of the feldspar samples. In our study, we have K-feldspar data from single crystals that mimic the types of data seen in classic resistance heater fusion experiments. Our step-heating data are based on using a continuous argon-ion laser with no direct control on temperature. However, with only a single added free parameter in the model, we show that it is possible to analyze this data in the multi-domain style, and make some simple inferences on the nature of the cooling history of the Carion pluton in central Madagascar. The Carion granitic pluton in central Madagascar was intruded into warm continental crust following orogenic events related to the final amalgamation of Gondwana. U-Pb SHRIMP dating of the pluton yields an emplacement age of 532.1 ± 2.1 Ma followed by relatively slow cooling as constrained by $^{40}Ar/^{39}Ar$ ages on hornblende, biotite and K-spar. Four hornblende samples yielded a mean $^{40}Ar/^{39}Ar$ age of 512.7 ± 1.3 Ma. A biotite sample yielded an age of 478.9 ± 1.0 Ma and modeled K-spar ages show cooling from 350° C at 466 Ma to 100° C by 410 Ma. Collectively, the data suggest that the pluton cooled from 850° C at 532.1 ± 5 (U-Pb zircon) Ma to 500° C at 512.7 ± 1.3 Ma ($^{40}Ar/^{39}Ar$ hornblende), or approximately 18 °C/Ma slowing to ~4 °C/Ma between 512 Ma and 478 Ma and finally to about 3°C/Ma between 478 and 410 Ma.

Key words: $^{40}Ar/^{39}Ar$ dating, Laser fusion, Gondwana, Madagascar, cooling history

1. Introduction

The island of Madagascar is located in a key position within the assembled Gondwana supercontinent (Figure 1). Geochronologic work in the past decade has provided important constraints on the evolution of the island (Paquette et al., 1994; Kröner et al., 1996; Ito et al., 1997; Paquette and Nedelec, 1998; Handke et al., 1999; Tucker et al., 1999a,b; Kröner et al., 2000). An excellent summary of these data is provided by Kröner et al. (2000).

Widespread magmatic activity in central Madagascar (granitoid and gabbroic intrusions) is dated between 824-740 Ma (Handke et al., 1999; Tucker et al., 1999a,b; Kröner et al., 2000). Handke et al. (1999) concluded that the magmatism resulted from Andean-type subduction beneath central Madagascar. Paquette and Nedelec (1998) dated 'stratoid' granites in central Madagascar. They reported U-Pb zircon ages of 627-633 Ma and interpreted the emplacement of these rocks in a post-collision extensional tectonic setting (Nedelec et al., 1995, 2000). A 611.7 ± 1.7 Ma $^{40}Ar/^{39}Ar$ plateau age on biotite (in progress by the author) supports these ages. According to Paquette and Nedelec (1998), Madagascar collided with East Africa at about 650 Ma and underwent extensional collapse at roughly 630 Ma.

The island of Madagascar experienced widespread thermal overprinting during the 500-570 Ma interval (see Kröner et al., 2000 and references therein). Meert (1999) attributed these ages to a younger collision between Australo-Antarctica and Madagascar. Kröner et al. (2000) argued that the granulite facies metamorphism in central Madagascar formed during extensional collapse as did Collins et al. (2000), but the locations of age determinations delineating this 'collapse' are closely associated with major shear zones. In southern Madagascar (south of the Bongolava-Ranotsara shear zone), Paquette et al. (1995) report granulite metamorphic ages between 523 and 577 Ma. These ages were used to argue for a high-grade regional metamorphic event between 565-580 Ma with the younger ages representing a thermal fluid disturbance in the isotopic systematics following high-grade regional metamorphism. Similar ages were obtained for the southern Madagascar domains by Andriamarofahatra et al. (1990), Nicollet et al. (1997) and Montel et al. (1994, 1996).

2. Geological setting & Previous Geochronology

The Carion granitic massif is situated to the east of Antananarivo. It is ~20 km in diameter and its elliptical shape is deeply indented in the north-west (Fig. 2). The Carion massif was emplaced near the western border of the Angavo shear belt (Fig. 2a), a major Panafrican structure that

parallels the eastern coast of Madagascar (Windley et al., 1994). Near Antananarivo, the Angavo belt is characterized by north-south steep foliations and shallowly plunging lineations acquired in low-pressure granulitic conditions (Ralison et al., 1997; Ralison, 1998; Nédélec et al., 2000). Paquette & Nédélec (1998) proposed that this shear zone was active from 570-550 Ma as were other major N-S shear zones in southern Madagascar (Paquette et al., 1994; Kröner et al., 1996).

Lautel (1953) first noted the post-tectonic setting of the Carion granite. The porphyritic nature of the rocks helps define steeply dipping magmatic lineations/foliations. In fact, the steep lineations contrast sharply with gently dipping lineations of the nearby Angavo shear belt (Nédélec et al., 2000; Meert et al., 2001). Incipient high-temperature solid-state deformation features (elongate quartz grains with occasional chessboard subgrain patterns) are observed in thin sections, but no orthogneissification is observed. Foliations in the country rocks are parallel with the massif, except in the northern indentation, where they are crosscut by the intrusion. The Carion massif shows no contact metamorphism at its margins. All of these data support a post-tectonic setting, but also show that the time lag between the formation of the Angavo shear belt (and its associated granulitic metamorphism) and the emplacement of the Carion magmas was short. Therefore both Nédélec et al. (2000) and Meert et al. (2001) assigned a late-syn tectonic setting for the Carion pluton.

The first attempt to date the Carion pluton by Vachette & Hottin (1974) resulted in two Rb/Sr isochron ages of 682 Ma and 527 Ma. The older age is likely devoid of any geological significance, as it was calculated using non-cogenetic rocks along with the typical Carion porphyritic granite. Kröner et al. (1999) reported a U-Pb evaporation age of 556 ± 1.7 Ma for the Carion pluton, but the location of the sample placed it outside the archetypal Carion massif. Indeed, we suggested that the 556 ± 1.7 Ma age (Kroner et al., 1999) dates the timing granulite formation in the nearby Angavo shear belt rather than the emplacement age of the Carion pluton (Meert et al., 2001). Subsequent dating of the pluton by Kröner et al. (2000) yielded a Pb-Pb age of 537.6 ± 1.0 Ma. Meert et al. (2001) used SHRIMP U-Pb methods and obtained a concordant age of 532.1 ± 5.1 Ma that overlaps with the age obtained by Kröner et al. (2001). $^{40}Ar/^{39}Ar$ dating of hornblende and bitoite from the Carion pluton by Meert et al. (2001) yielded ages of 512.7 ± 1.3 Ma and 478.9 ± 1.0 Ma respectively. Estimates of the closure temperatures for the minerals were also given in that study. The closure temperature estimates were 850° ± 50° C (U-Pb zircon), 500° ± 50° C for hornblende ($^{40}Ar/^{39}Ar$) and 350° ± 50° C for biotite ($^{40}Ar/^{39}Ar$).

3. Geochemistry/Emplacement Conditions

The main petrographic type of the Carion massif is a dark grey porphyritic granitoid of intermediate composition that can be easily identified in the field. The pluton displays a rough normal zoning ranging from tonalitic compositions at the rim to granodioritic and, locally, monzogranitic, compositions at the centre. Most rocks are porphyritic and contain conspicuous feldspar megacrysts with an average length of 2.5 cm. These megacrysts are generally perthitic orthoclase or microcline; in the more mafic rocks, they can also be plagioclase. Feldspars, both as megacrysts and as interstitial grains, constitute half the volume of the rocks. Plagioclase is generally unzoned and restricted to compositions in the range An_{24}-An_{26}, but can be as low as An_{10} in the most differentiated granite. Quartz is always present. Ferro-magnesian minerals amount to 10-25% of the modal compositions. They are mainly edenitic hornblende and biotite, both with xMg = 0.6-0.7. Relict orthopyroxene is observed in a few samples. Accessory minerals are present in noticeable amounts. Magnetite, apatite and zicon are ubiquitous, whereas titanite characterizes the most evolved rocks.

Representative major and trace element analyses are given in table 1 (reproduced from Madison-Razanatseheno, 1998). SiO_2 contents range from 61.62% to 73.49%. Actually, intermediate compositions predominate and the highest value corresponds to late magmatic veins in the center of the massif. In the diagram A/NK vs A/CNK of Fig. 3a, the rocks are metaluminous following the classification of Shand (1947) or I-type after Chappell & White (1974). In the K_2O vs SiO_2 diagram (Fig. 3b), they plot in the field of the high-K calc-alkaline series after Le Maître et al. (1989) or in the field of the shoshonitic series after Rickwood (1989). This is consistent with the noticeable abundance of K-feldspar (and hence of K_2O), even in the less evolved compositions. According to Liégeois et al. (1998), the low Na_20 contents at around 3% counterbalancing the high K_2O contents point to a shoshonitic trend rather than to a high-K calc-alkaline one. The Carion massif has a distinct ferriferous nature as can be seen from the Mg/Mg + Fe vs B diagram of Fig. 3c.

Among the trace elements, Ba appears especially abundant (1000-2300 ppm), but behaves as a compatible element controlled by the abundance of K-spar. Sr and Rb contents also display quite high values. Zr and Ce contents (respectively 388-762 and 176-327 ppm) are much higher than in typical I-type rocks, in agreement with the shoshonitic nature of the Carion massif. These high field-strength elements are hosted by accessory minerals and their abundance likely points to the

high-temperature character of the Carion magmas. In the Rb vs (Y + Nb) discrimination diagram of Pearce et al. (1984), the rocks plot in the field of within-plate granitoids (Fig. 3d)

Although geochemical data alone should not be used to identify the tectonic setting of the rocks because the geochemistry of magmatic rocks is likely to be influenced by the source (Chappell & Stephens, 1988), we note that the geochemistry of the Carion massif is consistent with its late- to post-tectonic setting. Indeed, high-K calc-alkaline or shoshonitic magmatism occurred also late in the Hercynian orogen of western Europe (Pagel & Leterrier, 1980; Debon & Lemmet, 1989), as well as in the Himalayan orogen of Tibet (Miller et al., 1999).

Emplacement conditions

Taking into account the late- to post-tectonic setting, the pressure calculations presented by Nédélec et al. (2000) are good estimates to infer the depth of emplacement of the Carion massif. Using the Al-in-hornblende barometer of Anderson & Smith (1995), these authors obtained a value of 3.3 (± 0.3) kb from a sample located 20 kilometers east of Carion and a value of 3.2 (± 0.1) kb from a sample located in the peripheral part of the Carion massif. Therefore, it is concluded that the Carion massif was emplaced at a depth of around 10-11 kilometers corresponding to these pressure conditions.

4. $^{40}Ar/^{39}Ar$ laser dating of K-spar

All argon age analyses were performed using a VG1200S mass spectrometer equipped with a Daly detector operated in analog mode. Samples were step-heated using a Coherent INNOVA model 70 argon ion laser with a nominal maximum output power of 5W. All analyses were performed with a fully automated fusion system, with laser power being set under computer control. Step-heating durations were 60 seconds, and the total fusion plus gas clean-up time was 3 minutes. Laser fusion system blanks were monitored frequently (typically every 5-6 fractions) and were normally about $1x10^{-13}$, $3x10^{-13}$, $3x10^{-14}$, $3x10^{-14}$, and $5x10^{-12}$ mlSTP for masses 36 through 40 respectively. The irradiation standard used was hornblende MMHb-1 with an assumed K-Ar age of 520.4 Ma (Samson and Alexander, 1987). Each irradiation consisted of a set of samples and standards sealed within evacuated fused silica tubes, and from each tube, at least 3 analyses for each of 5 packets

of MMHb-1 were analyzed. The resulting values of *J* were interpolated for each unknown sample location. Error estimates for *J* include scatter about the interpolation function. Mass discrimination in the mass spectrometer was monitored daily by analyzing an aliquot of atmospheric argon with a volume of about $5x10^{-9}$ mlSTP. Results are summarized in Table 2. Sample CAR-31 was taken from the center of the pluton (see Figure 2). Samples used in the previous study are also shown in Figure 2.

Since the late 1980's, it has been hypothesized that the wide range of apparent argon ages seen within single K-feldspar samples might be due to a distribution of diffusion domain sizes within the mineral. To test and apply this idea, an analytical technique which combines laboratory degassing experiments with numerical inversion procedures has been developed to extract cooling history information from feldspars (e.g. Lovera et al., 1989; Lovera et al., 1991). A key part of the method involves careful control of temperature in the laboratory to constrain the diffusion parameters of the feldspar samples. In our study, we have K-feldspar data from single crystals that mimic the types of data seen in classic resistance heater fusion experiments. Unfortunately, our step-heating data are based on using a continuous argon-ion laser with no direct control on temperature. However, with only a single added free parameter in the model, it may be possible to analyze this data in the multi-domain style, and make some simple inferences on the nature of the cooling history for the Carion granite.

The basic assumption to convert laser power into a proxy for temperature involves the mechanism for heat loss for a sample which is being laser step-heated. Hall et al. (1988) demonstrated, using data from an infra-red pyrometer, that to a very good approximation, cooling of a heated mineral grain in a UHV vacuum system could be accounted for simply via black-body radiation, and that thermal losses from conduction were negligible. Given this assumption, sample

temperature at steady state will be determined by a balance of laser power absorption and black-body radiation. Therefore, using the Stefan-Boltzmann law, the relationship between laser power and temperature can be written as:

$$aP = T^4 - T_0^4 \quad (1)$$

where P is laser power, T is absolute temperature, and T_0 is ambient temperature. The parameter α is a proportionality constant that will depend on the sample's reflectivity, emissivity, grain size, opacity, the laser beam size and other details of the system's optics. It is not possible to assign α accurately from first principles, but given the expected degassing temperatures for K-feldspars (400°-1100° C) and the actual laser powers used, we can roughly estimate that, for our experiments, α should have values of about 2 - 3 $x10^9$ with P measured in mW and T in Kelvin.

To model the ^{39}Ar release pattern, we used a modified version of the algorithm described in Hall (1990). In this method, the cumulative argon release pattern is fitted directly in the least squares sense, using a discrete suite of allowed domains. The problem is constrained by the fact that the contribution of each domain must be non-negative, and the total of all contributions must add up to one. This is a standard problem in quadratic programming and the specific algorithm used was adapted from Mifflin (1978). The suite of possible domains was a uniformly distributed set of 251 discrete domains having blocking temperatures (Dodson, 1973) ranging from 100° C to 350° C, using infinite slab geometry and assuming a cooling rate at blocking of 3 °C/Ma. Therefore, the allowed domain set had a temperature resolution of 1°C, which should be adequate for describing any reasonable set of actual domains. Using this method with resistance heater data, it can be shown that a broad range of diffusion activation energies can be made to fit laboratory data, as was argued by York and Hall (1990). Given that, plus the fact that we do not have direct laboratory temperature estimates, it was felt that it would not be possible to estimate this parameter from

our data and instead, a typical value for K-feldspar of 50 kcal/mol was assumed. That value, plus the constant α were the two free parameters in the fit of ^{39}Ar release. The maximum blocking temperature of 350° C was constrained by the fact that the K-feldspar ages are lower than the co-existing biotite ages, and 350° C is a reasonable blocking temperature estimate for our biotite as described by Meert et al. (2001).

Once the argon release pattern had been fit, the resulting set of domains with non-zero volume contributions were assigned argon blocking ages in order to fit the measured apparent age spectra. This was done assuming monotonic cooling from temperatures above the maximum allowed blocking temperature, and allowance was made for possible disturbances of each domain's age spectrum because of slow cooling through the blocking temperature. This correction used a method similar to that outlined in Onstott et al. (1989) and York (1984). The resulting age-temperature pairs can then be used as the basis for constructing a possible cooling history for the sample. Of course, the derived cooling trajectory is not the only possible cooling history that can fit the data; multiple episodes of reheating and argon loss are also possible. However, the fitted cooling trajectory will be close to the lowest possible cooling rates that can fit the data.

The K-feldspar data and the model fits to the age spectra (both ages and ^{39}Ar release) are shown in Figs. 4a-d. For both analyses, we show a range of models assuming a variety of α values. As can be seen from figures 4c,d , there the entire range of likely α values can give a very good fit to the data. The blocking age and blocking temperature pairs for the model domains are plotted in figures 5a,b. For both samples, the models show a cooling from about 350° C to about 200° C by about 430-440 Ma, with cooling to about 100° C by roughly 410 Ma. In figure 5c we show a possible composite series of blocking ages, with an α value for both samples of $2.8x10^9$. As can be seen from figure 5c, the models are broadly compatible with a cooling trend from 350° C at 480 Ma at a rate

of about 3-4° C/Ma. We stress that this model is non-unique and it is not required by the data. It is, however, perfectly compatible with the data.

5. Conclusions

Domain diffusion models of K-feldspar are frequently used to derive cooling trends of the host rock. These methods rely on resistance oven measurements with a direct control on laboratory temperatures. We show that with the addition of a single free parameter in the diffusion equation, laser step heated K-spar can be modelled in a similar fashion to conventional heating. This method was applied to a late-syn tectonic pluton in Madagascar and figure 5c shows the cooling history of the Carion pluton derived from the modelled K-spar data and previously published U-Pb, hornblende and biotite $^{40}Ar/^{39}Ar$ data. Initial cooling following zircon cystallization is ~18° C/Ma slowing to less than 5° C/Ma between 512 and 478 Ma and finally to about 3°C/Ma until roughly 410 Ma. This slow-cooling is consistent with the idea that the Carion granite intruded warm continental crust near the end of final Gondwana assembly (Meert et al., 2001) and suggests that laser step-heating of K-spar is a potentially viable means of constructing thermal histories of igneous plutons.

Acknowledgements

The authors wish to thank Chad Pullen for his help in the field and assistance in the laboratory, Marcus Johnson at the University of Michigan for running the Ar-Ar samples, Les Lezards de Tana for logistical support in the field. Financial support was provided through the National Science Foundation grant EAR98-05306 and by a US-Norway Fulbright Fellowship to JGM. A.N. received financial support from INSU-Intérieur de la Terre Program and CNRS-NSF program. Whole rock analyses were performed at the University of Bonn (Germany) with the cooperation of Prof. M. Raith.

Reference List

Anderson, J.L. and Smith, D.R., 1995, The effects of temperature and oxygen fugacity on the Al-in-hornblende barometer, Am. Mineral., 80, 549-559.

Berger, G.W. and York, D., 1981a, Geothermometry from $^{40}Ar/^{39}Ar$ dating experiments, Geochim. Cosmochim. Acta, 45, 795-811.

Chappell, B.W. & Stephens, W.E., 1988. Origin of infracrustal (I-type) granite magmas. Trans. Roy. Soc. Edinburgh, 79, 71-86.

Chappell, B.W. & White, A.J.R., 1974. Two contrasting granite types. Pacific Geol., 8, 173-174.

Debon, F. & Lemmet, M., 1999. Evolution of Mg/Fe ratios in Late Variscan plutonic rocks from the external crystalline massifs of the Alps (France, Italy, Switzerland). J. Petrol., 40, 1151-1185.

Dodson, M.H., 1973, Closure temperature in cooling geochronological and petrological systems, Contrib. Mineral. Petrol., 40, 259-279.

Hall, C.M., A method for estimating diffusion parameters and thermal histories from K-spar $^{40}Ar/^{39}Ar$ data, EOS Trans. Am. Geophys. U., 43, p.1297, 1990.

Hall, C.M., J.D. Redman, P.W. Layer and D. York, 1988, $^{40}Ar/^{39}Ar$ Ages from a Fully Automated Laser Microprobe, EOS Trans. Am. Geophys. U., 69, p. 520.

Handke, M.J., Tucker, R.D. and Ashwal, L.D., 1999, Neoproterozoic continental arc magmatism in west-central Madagascar, Geology, 27, 351-354.

Holland, T. and Blundy, J., 1994, Non-ideal interactions in calcic-amphiboles and their bearing on amphibole-plagioclase thermometry, Contr. Mineral. Petrol., 116, 433-447.

Kröner, A., Windley, B.F., Jaeckel, P., Brewer, T.S., Nemchin, A. and Razakamanana, T., 1999, New zircon ages and regional significance for the evolution of the Pan-African orogen in Madagascar, J. Geol. Soc. London, 156, 1125-1135.

Kröner, A., Braun, I. & Jaeckel, P., 1996. Zircon geochronology of anatectic melts and residues from a high-grade pelitic assemblage at Ihosy, southern Madagascar: evidence for Pan-African granulite metamorphism. Geol. Mag., 133, 311-323.

Lautel, R., 1953. Etude géologique du socle cristallin à la latitude de Tamatave. Ph. D. Thesis, Univ. Clermont-Ferrand (France).

Le Maître, R.W. et al., 1989. A classification of igneous rocks and glossary of terms. Balckwell, Oxford.

Liégeois, J.P., Navez, J., Hertogen, J. & Black, R., 1998. Contrasting origin of post-collisional high-K calcalkaline and shoshonitic versus alkaline and peralkaline granitoids - the use of sliding normalization. Lithos, 45, 1-28.

Lovera, O.M., Richter, F.M. and Harrison, T.M., 1989, The $^{40}Ar/^{39}Ar$ thermochronometry for slowly cooled samples having a distribution of diffusion domain sizes, J. Geophys. Res., 94, 17917-17935.

Lovera, O.M., Richter, F.M. and Harrison, T.M., 1991, Diffusion domains determined by ^{39}Ar released during step heating, J. Geophys. Res., 96, 2057-2069.

Madison Razanatseheno, M. O., 1998, Granite de Carion: Approches petrologiques et structurales (M.Sc. thesis), Unverisite d'Antananarivo, 61 pp.

Martelat, J.E., Lardeaux, J.M., Nicollet, C. & Rakotondrazafy, R., 1999 (?). Strain pattern and late precambrian deformation history in southern Madagascar. Precambrian Res., in press.

McDougall, I. and T. M. Harrison, 1999, Geochronology and Thermochronology by the $^{40}Ar/^{39}Ar$ method, Oxford University Press, Oxford, 269 pp.

Meert, J.G., Nedelec, A., Hall, C.M., Wingate, M.T.D. and Rakotondrazafy, M., 2001, Paleomagnetism, geochronology and tectonic implications of the Carion granite, Madagascar, Tectonophys., in press.

Mifflin, R., A feasible descent algorithm for linearly constrained least squares problems, 1978, in Nonsmooth optimization: Proceedings of a IIASA workshop March 28-April 8 1977, eds. C. Lemarechal and R. Mifflin, Pergamon Press, Oxford.

Miller, C., Schuster, R., Klötzli, U., Franck, W. & Purtscheller, F., 1999. Post-collisional potassic and ultrapotassic magmatism in SW Tibet: geochemical and Sr - Nd - Pb - O isotopic constraints for mantle source characteristics and petrogenesis. J. Petrol., 40, 1399-1424.

Nédélec, A. Stephens, W.E. and Fallick, A.E., 1995, The Panafrican stratoid granites of Madgascar: Alkaline magmatism in a post-collisional extensional setting, J. Petrol., 36, 1367-1391.

Nédélec, A., Ralison, B., Bouchez, J.L. & Grégoire, V., 2000, Structure and metamorphism of the granitic basement around Antananarivo: a key to the Panafrican history of central Madagascar and its Gondwana connections. Tectonics, in press.

Onstott, T.C., Hall, C.M. and York, D., 1989, $^{40}Ar/^{39}Ar$ thermochronometry of the Imataca complex, Venezuela, Precambrian Res., 42, 255-291.

Pagel, M. & Leterrier, J., 1980. The subalkaline potassic magmatism of the Ballons massif (Southern Vosges, France): shoshonitic affinity. Lithos, 13, 1-10.

Paquette, J.L. & Nédélec, A., 1998. A new insight into Panafrican tectonics in the East-West Gondwana collision zone by U-Pb zircon dating of granites from central Madagascar. Earth Planet. Sci. Lett., 155, 45-56, 1998.

Paquette, J.L., Nédélec, A., Moine, B. & Rakotondrazafy, M., 1994. U-Pb, single zircon evaporation and Sm-Nd isotopic study of a granulitic domain in SE Madagascar. J. Geol., 102, 523-538.

Pearce, J.A., Harris, N.B.W. & Tindle, A.G., 1984. Trace element discrimination diagrams for the tectonic interpretation of granitic rocks. J. Petrol., 25, 956-983.

Ralison, B., 1998, Structure et pétrologie du socle panafrican dans la region d'Antananarivo: implications géodynamiques, Ph.D. thesis, University of Antananarivo, Madagascar, 130 pp.

Ralison, B. and Nédélec, A., 1997, Contrasted Pan-African structures near Antananarivo, Madagascar, Symposium IGCP-UNESCO Antananarivo, abstr. P 83-84.

Rickwood, P.C., 1989. Boundary lines within petrologic diagrams which use oxides of major and minor elements. Lithos, 22, 247-263.

Samson, S.D. and Alexander, E.C., 1987, Calibration of the interlaboratory ^{40}Ar-^{39}Ar dating standard, Mmhb-1. Chem. Geol., 66, 27-34.

Sengupta, P., Dasgupta, S., Bhattacharya, P.K. and Mukharjee, M., 1994, An orthopyroxene-biotite geothermometer and its application in crustal granulites and mantle-derived rocks, J. Metamorph. Geol., 8, 191-197.

Shand, S.J., 1947. Eruptive rocks. Their genesis, composition, classification, and their relation to ore-deposits (3rd edition). J. Wiley, New York, 488 p.

Tucker, R.D., Ashwal, L.D., Handke, M.J., Hamilton, M.A., LeGrange, M. and Rambeloson, R.A., 1999, U-Pb geochronology and isotope geochemistry of Archean and Proterozoic rocks of north-central Madagascar, J. Geol., 107, 135-154.

Vachette, M.& Hottin, A.M., 1974. Ages de 682 et 527 Ma dans le massif granitique de Carion (Centre de Madagascar). C. R. Acad. Sci. Paris, 278, 1669-1671.

Windley, B.F., A. Razafiniparany, T. Razakamanana and D. Ackermand, 1994. Tectonic framework of the Precambrian of Madagascar and its Gondwana connections: a review and reappraisal. Geol. Rundsch., 83, 642-659.

York, D. and Hall, C.M., Sensitivity of $^{40}Ar/^{39}Ar$ derived thermal histories to diffusion parameter estimates, EOS Trans. Am. Geophys. U., 43, p.1297, 1990.

York, D., 1984, Cooling Histories from ^{40}Ar /^{39}Ar Age Spectra: Implications for Precambrian Plate Tectonics, Ann. Rev. Earth Planet. Sci., 12, 384-409.

Table 1. Selected Geochemical Analyses from the Carion Massif

Element (wt %)	GC 24	GC 6	GC 3	GC 20	GC 14	GC 25	GC 12
SiO2	61.62	62.26	62.52	65.13	65.92	66.68	70.49
TiO2	1.33	1.51	1.42	1.17	1.06	1.02	0.62
Al2O3	15.09	14.17	14.67	14.19	14.55	13.98	12.67
FeO	5.76	6.24	6.07	5.02	4.7	4.46	2.57
MnO	0.06	0.09	0.08	0.07	0.07	0.04	0.04
MgO	1.57	1.67	1.64	1.31	1.31	1.05	0.52
CaO	3.72	3.59	3.75	3.05	2.76	2.42	1.47
Na2O	3.28	3.21	3.38	3.16	3.32	2.95	2.98
K2O	4.42	4.47	4.47	4.87	4.95	4.78	4.87
P2O5	0.62	0.69	0.66	0.5	0.47	0.45	0.2
SO3	0.05	0.06	0.06	0.05	0.04	0.04	0.02
l.i.	0.40	0.00	0.00	0.00	0.00	0.50	0
Total	98.78	99.14	99.86	99.51	100.03	99.06	99.99
(ppm)							
Ba	2303	2293	2331	2018	2044	1998	1078
Rb	110	85	108	124	130	123	122
Sr	741	682	704	588	554	585	319
Zr	592	762	650	734	537	696	388
Ce	222	308	225	332	241	327	176
Y	44	44	37	56	40	98	32
Nb	31	42	38	41	30	36	18

Table 2. Argon Results (Run A-CAR-31 K-spar)

Laser Power (mW)	Cum ^{39}K	$^{40}*Ar/^{39}K$	+/-	%Atmos	$^{37}Ca/^{39}K$	+/-	$^{40}Ar/^{36}Ar$	+/-	Age (Ma)	+/- (Ma)
50	2.28e-4	15.7	3.51	38.7	3.05e-2	2.33e-2	7.62e+2	2.67e+2	248.3	52.1
100	1.87e-3	29.6	.425	4.81	1.17e-2	3.52e-3	6.13e+3	1.64e+3	443.8	5.65
150	8.25e-3	26.4	.238	.817	1.269e-2	1.18e-3	3.61e+4	3.07e+4	401.6	3.23
200	1.96e-2	27.6	.077	.906	1.25e-2	6.83e-4	3.26e+4	7.46e+3	417.3	1.04
225	2.95e-2	27.9	.118	.483	1.105e-2	6.36e-4	6.11e+4	3.84e+4	421.1	1.59
250	3.92e-2	28.2	.135	.156	1.11e-2	6.63e-4	6.10e+4	3.76e+5	425.1	1.81
275	4.92e-2	28.0	.157	.866	9.37e-3	5.43e-4	3.41e+4	1.83e+4	422.9	2.11
300	5.87e-2	28.3	.117	.118	8.46e-3	6.46e-4	2.48e+5	6.03e+5	426.6	1.56
325	6.75e-2	28.2	.132	.632	8.21e-3	6.28e-4	4.67e+4	2.33e+4	424.4	1.78
350	7.55e-2	28.2	.129	5.80	7.51e-3	6.70e-4	5.09e+3	3.08e+2	425.1	1.73
375	8.29e-2	28.7	.100	.590	6.77e-3	5.18e-4	5.00e+4	2.19e+4	432.1	1.33
400	8.95e-2	29.1	.116	.400	8.32e-3	8.37e-4	7.39e+4	5.77e+4	436.9	1.54
450	9.74e-2	29.2	.145	.318	7.23e-3	7.06e-4	9.27e+4	1.09e+5	438.0	1.95
500	1.04e-1	30.3	.263	----	6.67e-3	9.52e-4	-----	-----	452.4	3.48
550	1.11e-1	30.3	.158	----	5.62e-3	1.22e-3	-----	-----	452.7	2.09
600	1.18e-1	30.8	.115	----	7.46e-3	8.71e-4	-----	-----	460.4	1.51
650	1.26e-1	30.9	.136	.017	8.65e-3	8.29e-4	1.69e+6	3.41e+7	461.7	1.79
700	1.37e-1	31.2	.093	----	9.62e-3	7.81e-4	-----	-----	464.9	1.22
800	1.57e-1	31.1	.090	----	9.00e-3	3.53e-4	-----	-----	462.9	1.20
900	1.92e-1	30.9	.220	.230	8.37e-3	2.45e-4	1.28e+5	7.54e+4	461.3	2.89
950	2.23e-1	31.0	.068	.187	8.01e-3	1.85e-4	1.57e+5	8.67e+4	462.7	.899
1000	2.52e-1	31.2	.050	.068	7.59e-3	2.57e-4	4.32e+5	6.91e+5	464.3	.667
1050	2.81e-1	31.2	.049	.135	7.34e-3	3.13e-4	2.18e+5	1.63e+5	464.4	.649
1100	3.08e-1	31.3	.068	.144	7.35e-3	2.56e-4	2.05e+5	1.66e+5	465.8	.889
1150	3.35e-1	31.4	.063	.137	6.96e-3	1.92e-4	2.15e+5	1.57e+5	467.1	.829
1200	3.61e-1	31.3	.049	.195	6.86e-3	2.07e-4	1.51e+5	1.02e+5	465.6	.637
1250	3.87e-1	31.3	.057	.121	6.91e-3	2.34e-4	2.43e+5	2.52e+5	465.8	.751
1300	4.13e-1	31.3	.067	.260	6.92e-3	2.56e-4	1.14e+5	5.21e+4	466.1	.885
1350	4.38e-1	31.4	.052	.165	6.85e-3	1.62e-4	1.79e+5	1.28e+5	466.8	.682
1400	4.64e-1	31.4	.055	.088	6.88e-3	1.84e-4	3.35e+5	3.43e+5	467.8	.722
1450	4.88e-1	31.4	.076	.219	6.96e-3	1.99e-4	1.35e+5	7.42e+4	467.4	.995
1500	5.16e-1	31.5	.078	.053	6.62e-3	2.78e-4	5.51e+5	1.11e+6	468.5	1.02
1550	5.47e-1	31.5	.052	----	6.17e-3	2.19e-4	-----	-----	469.0	.683
1600	5.74e-1	31.4	.070	.254	6.55e-3	2.69e-4	1.16e+5	6.17e+4	467.7	.917
1650	6.00e-1	31.6	.068	----	5.69e-3	3.11e-4	-----	-----	470.5	.896
1700	6.27e-1	31.4	.047	.122	6.87e-3	2.02e-4	2.41e+5	2.62e+5	467.7	.639
1750	5.58e-1	31.6	.043	.024	5.91e-3	2.17e-4	1.22e+6	4.68e+6	469.5	.568
1800	6.83e-1	31.6	.055	.085	5.85e-3	2.90e-4	3.47e+5	3.60e+5	470.2	.720
1850	7.06e-1	31.5	.063	.187	6.05e-3	2.60e-4	1.58e+5	1.16e+5	469.2	.827
1900	7.30e-1	31.5	.073	.357	5.99e-3	4.28e-4	8.27e+4	4.21e+4	468.4	.960
2000	7.79e-1	31.6	.041	.514	5.91e-3	2.61e-4	5.75e+4	9.91e+3	470.0	.542
2050	7.97e-1	31.5	.074	.524	6.01e-3	3.81e-4	5.64e+4	1.59e+4	468.8	.976
2100	8.15e-1	31.6	.083	.323	6.00e-3	3.34e-4	9.15e+4	3.05e+4	469.7	1.08
2200	8.42e-1	31.6	.074	.164	5.71e-3	2.92e-4	1.79e+5	2.11e+5	470.3	.964
2300	8.77e-1	31.7	.033	.030	5.41e-3	1.92e-4	9.99e+5	2.22e+6	471.8	.423
2400	8.83e-1	32.0	.176	----	5.82e-3	1.18e-3	-----	-----	475.7	2.30
2500	9.08e-1	31.8	.062	.057	5.67e-3	2.62e-4	5.82e+5	1.21e+6	472.6	.807
2600	9.09e-1	30.3	1.71	7.30	1.67e-2	1.34e-2	4.04e+3	2.84e+3	454.3	22.7
2700	9.09e-1	32.7	1.28	----	2.66e-2	1.66e-2	-----	-----	484.7	16.7
2800	9.10e-1	33.3	.726	----	-----	-----	-----	-----	493.2	9.4
3600	1.00e+0	32.0	.039	.127	5.46e-3	1.16e-4	2.31e+5	6.35e+4	475.4	.508

Table 2. Argon Results (Run B CAR-31a Kspar)

Laser Power (mW)	Cum ^{39}K	$^{40}*Ar/^{39}K$	+/-	%Atmos	$^{37}Ca/^{39}K$	+/-	$^{40}Ar/^{36}Ar$	+/-	Age (Ma)	+/- (Ma)
50	1.83e-4	22.1	4.54	35.0	1.48e-1	7.73e-2	8.43e+2	3.16e+2	324.5	63.9
100	1.10e-3	27.1	1.04	9.59	6.48e-2	1.61e-2	3.08e+3	1.10e+3	410.8	14.1
150	5.82e-3	27.1	.232	2.08	1.18e-1	3.30e-3	1.42e+4	4.92e+3	410.2	3.14
200	1.96e-2	27.9	.091	.675	4.00e-2	1.19e-3	4.38e+4	1.88e+4	421.7	1.22
225	3.21e-2	28.4	.104	.879	2.66e-2	1.18e-3	3.36e+4	1.32e+4	427.7	1.39
250	4.54e-2	28.7	.078	.328	3.06e-2	1.33e-3	8.98e+4	6.68e+4	431.9	1.04
275	5.84e-2	28.5	.086	.061	3.38e-2	1.02e-3	4.83e+5	2.07e+6	429.9	1.14
300	7.15e-2	28.8	.102	.274	3.51e-2	1.19e-3	1.08e+5	1.16e+5	432.9	1.36
325	8.56e-2	28.9	.092	.448	3.79e-2	1.15e-3	6.68e+4	3.45e+4	435.3	1.23
350	9.98e-2	28.8	.184	.377	3.62e-2	9.31e-4	7.82e+4	5.16e+4	433.4	2.47
375	1.13e-1	28.9	.106	----	3.40e-2	1.50e-3	-----	-----	434.7	1.41
400	1.28e-1	29.3	.239	.394	3.39e-2	2.16e-3	7.48e+4	1.52e+5	439.6	3.19
450	1.46e-1	29.4	.181	1.46	3.32e-2	1.66e-3	2.09e+4	7.41e+3	440.7	2.40
500	1.66e-1	29.5	.148	.781	3.17e-2	1.52e-3	3.78e+4	2.35e+4	442.0	1.98
550	1.86e-1	29.7	.117	.294	2.94e-2	1.3e-3	1.00e+5	1.28e+5	445.0	1.55
600	2.06e-1	29.8	.142	1.38	2.56e-2	1.58e-3	2.13e+4	6.57e+3	445.7	1.88
650	2.24e-1	29.9	.127	1.35	2.16e-2	1.39e-3	2.17e+4	6.21e+3	447.4	1.69
700	2.42e-1	30.5	.153	.992	2.04e-2	1.36e-3	2.97e+4	1.45e+4	455.7	2.03
750	2.62e-1	30.6	.110	.779	1.78e-2	1.16e-3	3.79e+4	1.67e+4	456.3	1.45
800	2.79e-1	30.6	.187	.776	1.73e-2	1.17e-3	3.81e+4	2.94e+4	456.5	2.47
850	2.95e-1	30.8	.191	.384	1.48e-2	1.42e-3	7.67e+4	1.18e+5	459.2	2.52
900	3.13e-1	31.3	.200	.166	1.27e-2	1.58e-3	1.77e+5	6.59e+5	466.6	2.62
950	3.31e-1	31.2	.189	.413	1.58e-2	1.54e-3	7.15e+4	9.88e+4	464.8	2.49
1000	3.52e-1	31.0	.199	----	1.56e-2	1.18e-3	-----	-----	462.4	2.63
1050	3.77e-1	30.9	.109	.405	1.43e-2	1.08e-3	7.29e+4	5.46e+4	460.7	1.43
1100	3.99e-1	30.7	.126	.702	1.59e-2	1.41e-3	4.21e+4	2.25e+4	458.9	1.65
1150	4.24e-1	30.8	.141	.808	1.67e-2	1.17e-3	3.65e+4	1.89e+4	459.8	1.85
1200	4.51e-1	30.8	.130	.534	1.64e-2	1.16e-3	5.53e+4	4.28e+4	460.0	1.71
1250	4.79e-1	30.9	.116	.346	1.64e-2	1.19e-3	8.53e+4	8.51e+4	460.6	1.53
1300	5.08e-1	30.8	.129	.844	1.58e-2	1.36e-3	3.50e+4	1.60e+4	459.2	1.70
1350	5.37e-1	30.8	.111	.510	1.34e-2	1.17e-3	5.79e+4	3.59e+4	459.8	1.46
1400	5.65e-1	30.9	.139	.725	1.41e-2	1.24e-3	4.07e+4	2.34e+4	460.8	1.83
1450	5.92e-1	30.9	.111	.438	9.87e-3	8.46e-4	6.75e+4	4.68e+4	461.6	1.46
1500	6.18e-1	30.8	.095	.671	9.34e-3	9.78e-4	4.40e+4	1.68e+4	459.3	1.25
1550	6.43e-1	30.7	.113	.938	9.68e-3	1.03e-3	3.15e+4	1.16e+4	457.7	1.49
1600	7.60e-1	31.1	.081	.125	1.01e-2	1.72e-4	2.34e+5	1.58e+5	462.8	1.06
1650	7.91e-1	31.1	..097	.239	8.43e-3	6.29e-4	1.24e+5	1.53e+5	463.4	1.28
1700	8.08e-1	31.1	.198	.294	5.20e-3	1.09e-3	1.00e+5	2.11e+5	463.3	2.61
1750	8.21e-1	31.2	.244	.253	6.63e-3	8.53e-4	1.17e+5	3.42e+5	464.7	3.21
1800	8.29e-1	31.1	.236	.691	-----	-----	4.27e+4	4.21e+4	463.3	3.10
1850	8.37e-1	31.3	.293	.192	9.23e-4	2.28e-3	1.54e+5	7.16e+5	465.6	3.85
1900	8.44e-1	31.4	.303	.444	1.54e-3	4.38e-3	6.66e+4	1.34e+5	467.9	3.97
1950	8.50e-1	30.9	.325	2.46	2.07e-3	3.56e-3	1.20e+4	4.63e+3	460.8	4.27
2000	8.56e-1	31.6	.370	----	1.99e-3	4.23e-3	-----	-----	470.2	4.85
2100	8.62e-1	31.0	.467	1.26	4.00e-3	2.91e-3	2.35e+4	2.65e+4	462.2	6.14
2200	8.69e-1	30.9	.331	1.65	5.17e-3	2.07e-3	1.80e+4	1.09e+4	460.4	4.36
2300	8.77e-1	30.8	.251	1.94	5.68e-3	3.30e-3	1.52e+4	6.10e+3	459.1	3.31
2400	8.85e-1	31.5	.236	1.01	2.87e-3	2.15e-3	2.92e+4	1.95e+4	469.0	3.09
2600	8.91e-1	31.4	.320	.896	6.53e-3	3.47e-3	3.30e+4	3.27e+4	467.5	4.20
3000	8.95e-1	30.6	.425	4.00	-----	-----	7.38e+3	2.30e+3	456.8	5.61
3600	9.78e-1	31.8	.043	.312	7.33e-3	3.11e-4	9.48e+4	2.52e+4	472.3	.568
3601	9.90e-1	31.0	.166	1.18	1.43e-2	2.21e-3	2.50e+4	9.97e+3	461.8	2.2
3602	1.00	30.6	.340	1.85	1.68e-2	2.87e-3	1.59e+4	8.74e+3	456.8	4.49

Notes: ----- signifies (-) values below limits of machine. J-value 9.4201e-3 ± 2.96964e-5

Figure Legends

Figure 1: Paleogeographic map of Gondwana c. 510 Ma showing the position of Madagascar (based on Meert et al., 2001).

Figure 2: (a) Regional geologic setting of the Carion pluton in central Madagascar. The Angavo shear zone formed at ca. 550 Ma and was subsequently intruded by the post-tectonic to late syn-tectonic Carion pluton. (b) Sampling locations within the Carion pluton for geochemistry (labelled GC, see Table 1) and for geochronology (Hbl=hornblende $^{40}Ar/^{39}Ar$ ages; bt=biotite $^{40}Ar/^{39}Ar$ ages; K-spar=potassium feldspar $^{40}Ar/^{39}Ar$ ages; U-Pb=Uranium-Lead ages) see Meert et al., 2001 and Kroner et al., 2000.

Figure 3: (a) A/NK vs A/CNK diagram (b) K2O vs SiO2 diagram showing the limits of the fields of calc-alkaline and shoshonitic series after Le Maître et al. (1989): dotted lines, and Rickwood (1989): shaded areas. (c) Mg/Mg+Fe diagram of Debon & Lemmet (1999) and (d) Rb vs (Y+Nb) diagram of Pearce et al. (1984).

Figure 4: (a,b) Results from analyses of the K-feldspar sample CAR-31a. Figs (c) and (d) show the best fit multi-domain age spectral models for runs W0a and W0b respectively. Only data with laser powers < 2000 mW and less were fit, and the fractions above that level were combined into a single fraction. There is very little difference between models with different values of α.

Figure 5: (a-b) Plots of the multi-domain model domain closure temperatures (assuming slab geometry and cooling rate at blocking of 3 °C/Ma) for CAR-31a K-feldspar runs W0a and W0b. A range of a values for each run are shown. For comparison, the total gas age for biotite CAR-31a run V9a is shown with an assumed closure temperature of 350° C. In (c) is shown a combined set of domain closure temperatures, along with reference cooling lines from the biotite value at rates of 3, 3.5 and 4 °C/Ma. (d) Cooling history of the Carion pluton obtained from U-Pb and $^{40}Ar/^{39}Ar$ isotopic ages. Error bars reflect the uncertainty in age and closure temperature of the isotopic systems as described in the text or in Figure 5c (for K-spar model ages).

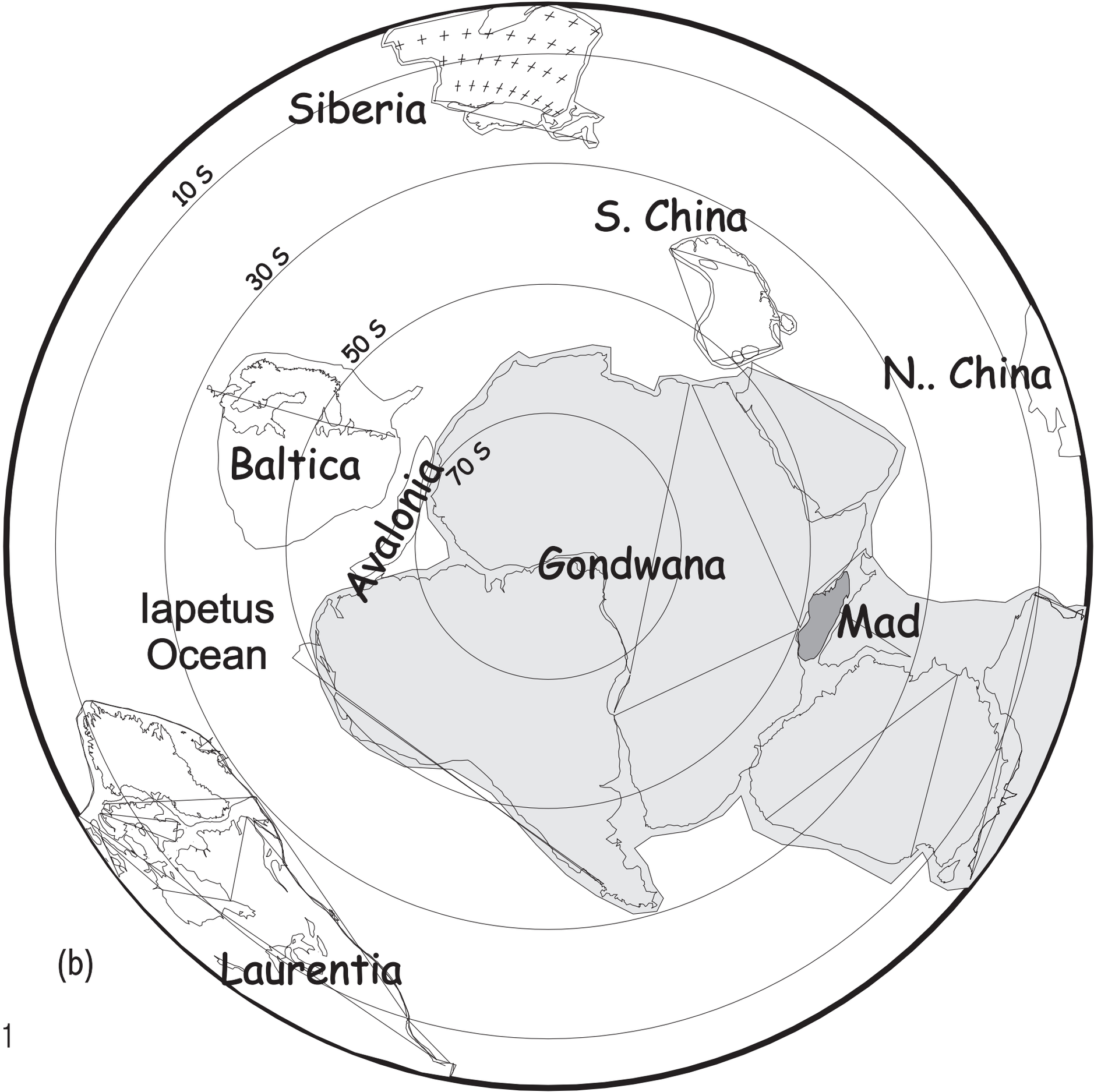
Siberia
10 S
30 S
50 S
70 S
S. China
N.. China
Baltica
Avalonia
Gondwana
Mad
Iapetus
Ocean
Laurentia
(b)

Fig 1

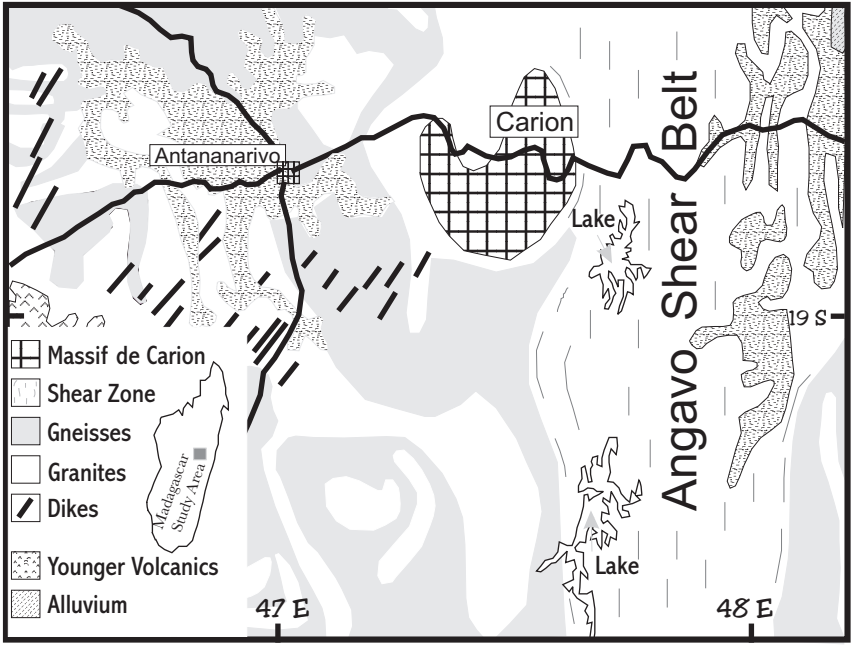
Antananarivo
Carion
Lake
Angavo Shear Belt
19 S
Massif de Carion
Shear Zone
Gneisses
Granites
Dikes
Younger Volcanics
Alluvium
Madagascar Study Area
Lake
47 E
48 E

(a)

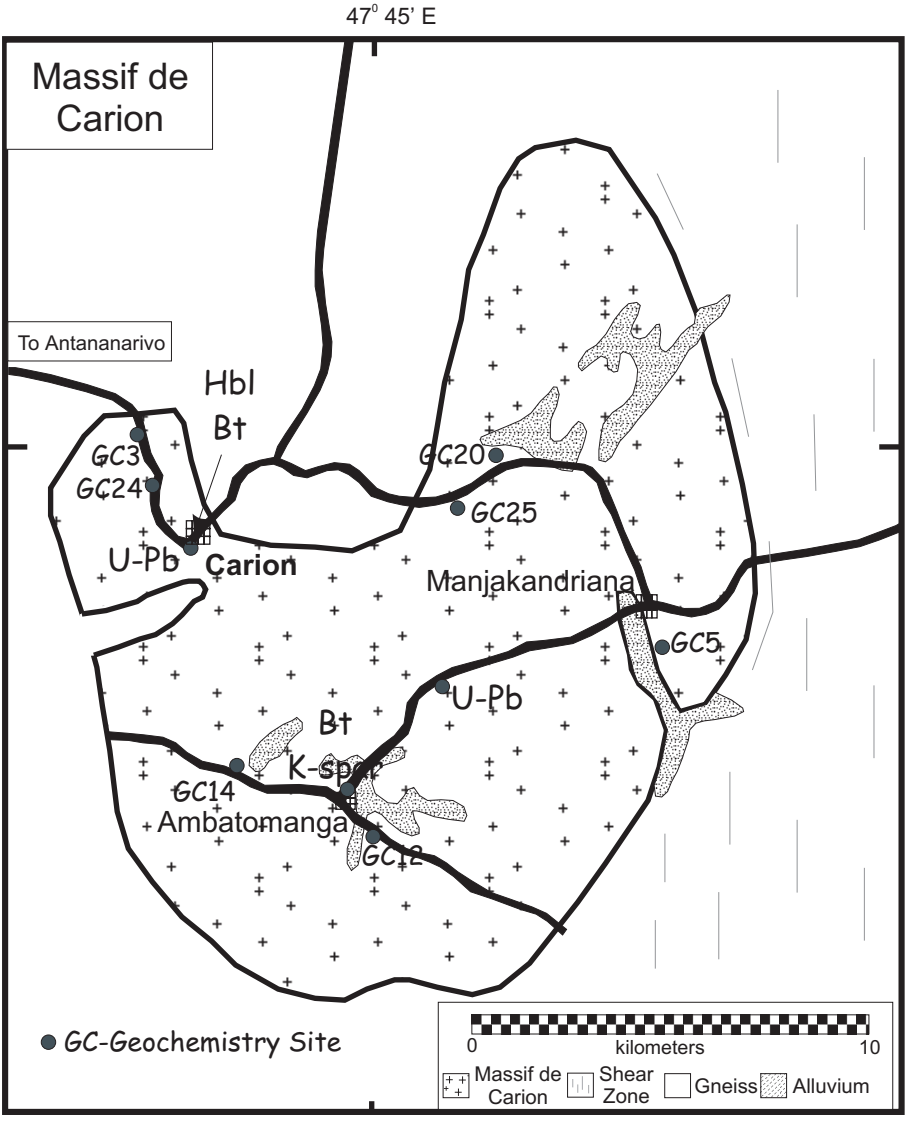
47° 45' E
Massif de Carion
To Antananarivo
Hbl
Bt
GC3
GC24
U-Pb
Carion
GC20
GC25
18° 50' N
Manjakandriana
GC5
U-Pb
Bt
K-spar
GC14
Ambatomanga
GC12
GC-Geochemistry Site
0
kilometers
10
Massif de Carion
Shear Zone
Gneiss
Alluvium
47° 45' E

Fig 2 (b)

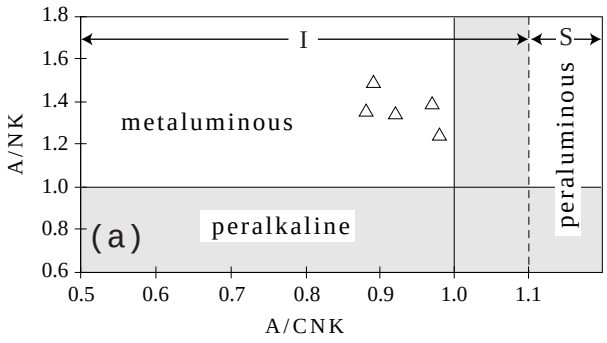
I
S
metaluminous
peraluminous
peralkaline
(a)
A/NK
A/CNK
1.8
1.6
1.4
1.2
1.0
0.8
0.6
0.5
0.6
0.7
0.8
0.9
1.0
1.1

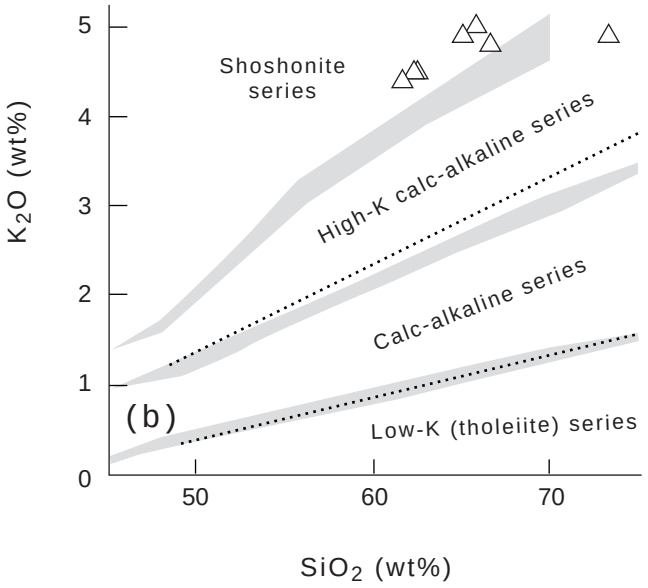
Shoshonite series
High-K calc-alkaline series
Calc-alkaline series
Low-K (tholeiite) series
(b)
K2O (wt%)
SiO2 (wt%)
5
4
3
2
1
0
50
60
70

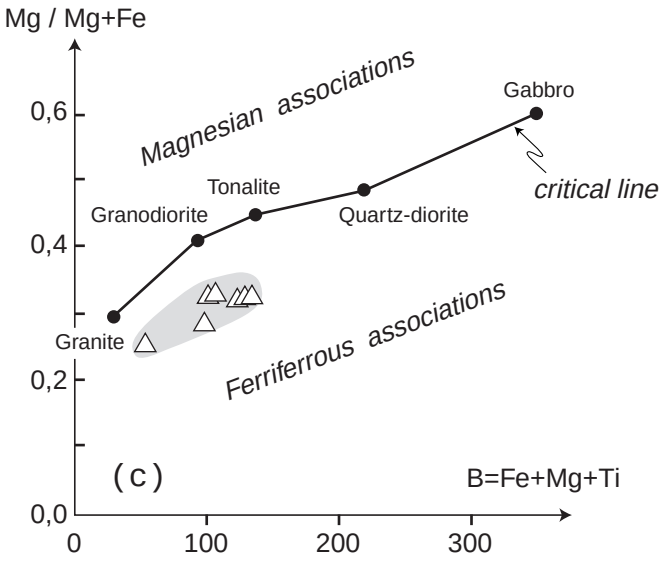
Mg / Mg+Fe
Magnesian associations
Ferriferrous associations
Gabbro
Tonalite
Granodiorite
Quartz-diorite
Granite
critical line
(c)
B=Fe+Mg+Ti
0,6
0,4
0,2
0,0
0
100
200
300

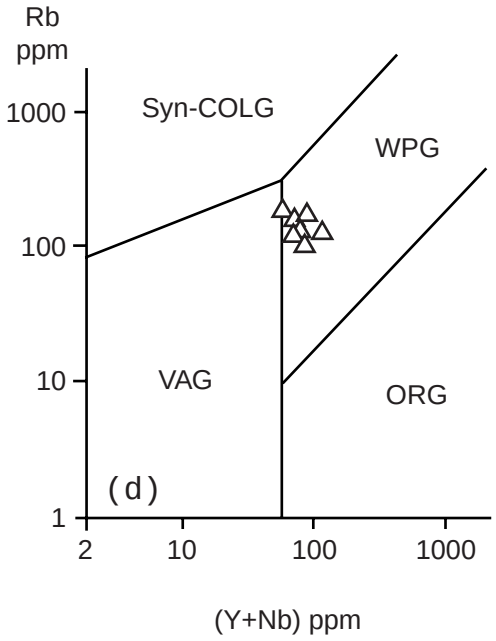
Rb ppm
Syn-COLG
WPG
VAG
ORG
(d)
(Y+Nb) ppm
1000
100
10
1
2
10
100
1000

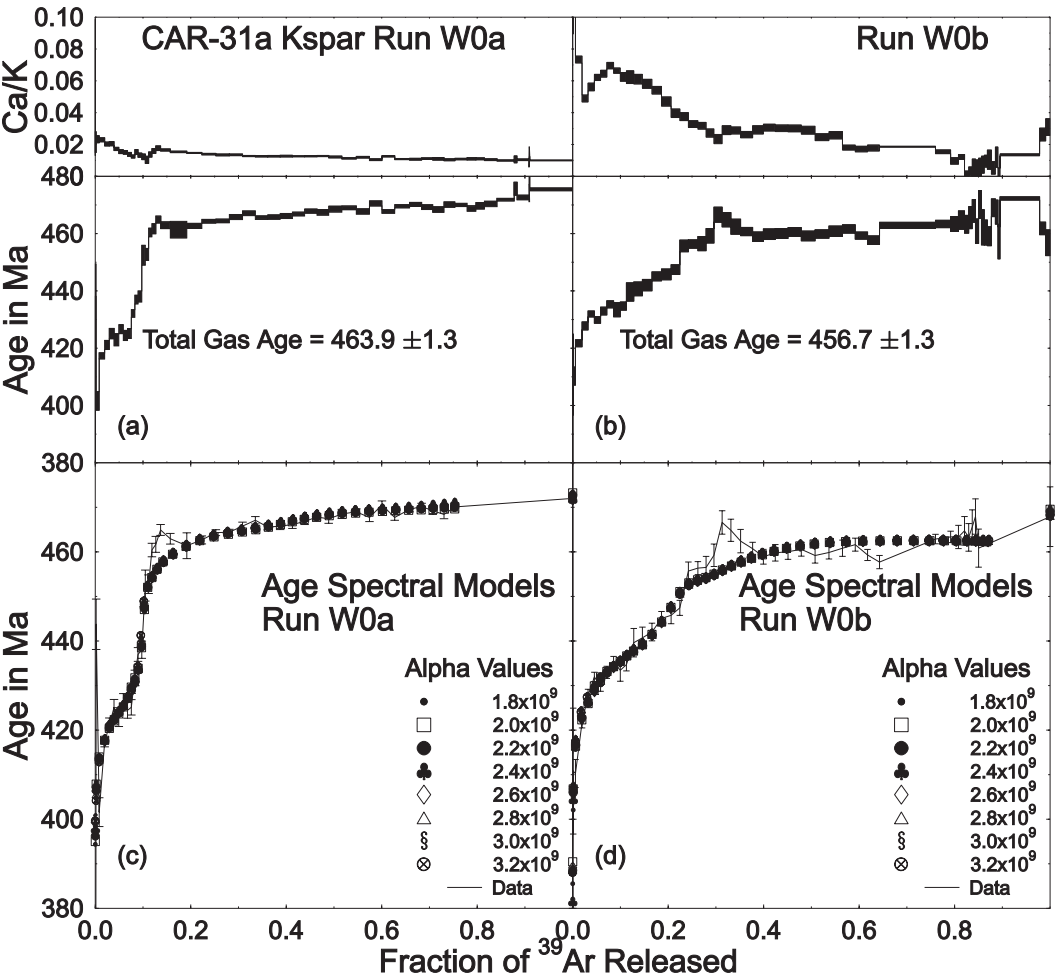
CAR-31a Kspar Run W0a
Run W0b
Ca/K
0.10
0.08
0.06
0.04
0.02
Age in Ma
480
460
440
420
400
380
Total Gas Age = 463.9 ±1.3
Total Gas Age = 456.7 ±1.3
(a)
(b)
Age Spectral Models
Run W0a
Age Spectral Models
Run W0b
Alpha Values
1.8x10^9
2.0x10^9
2.2x10^9
2.4x10^9
2.6x10^9
2.8x10^9
3.0x10^9
3.2x10^9
Data
(c)
(d)
0.0
0.2
0.4
0.6
0.8
Fraction of 39Ar Released

Fig.4

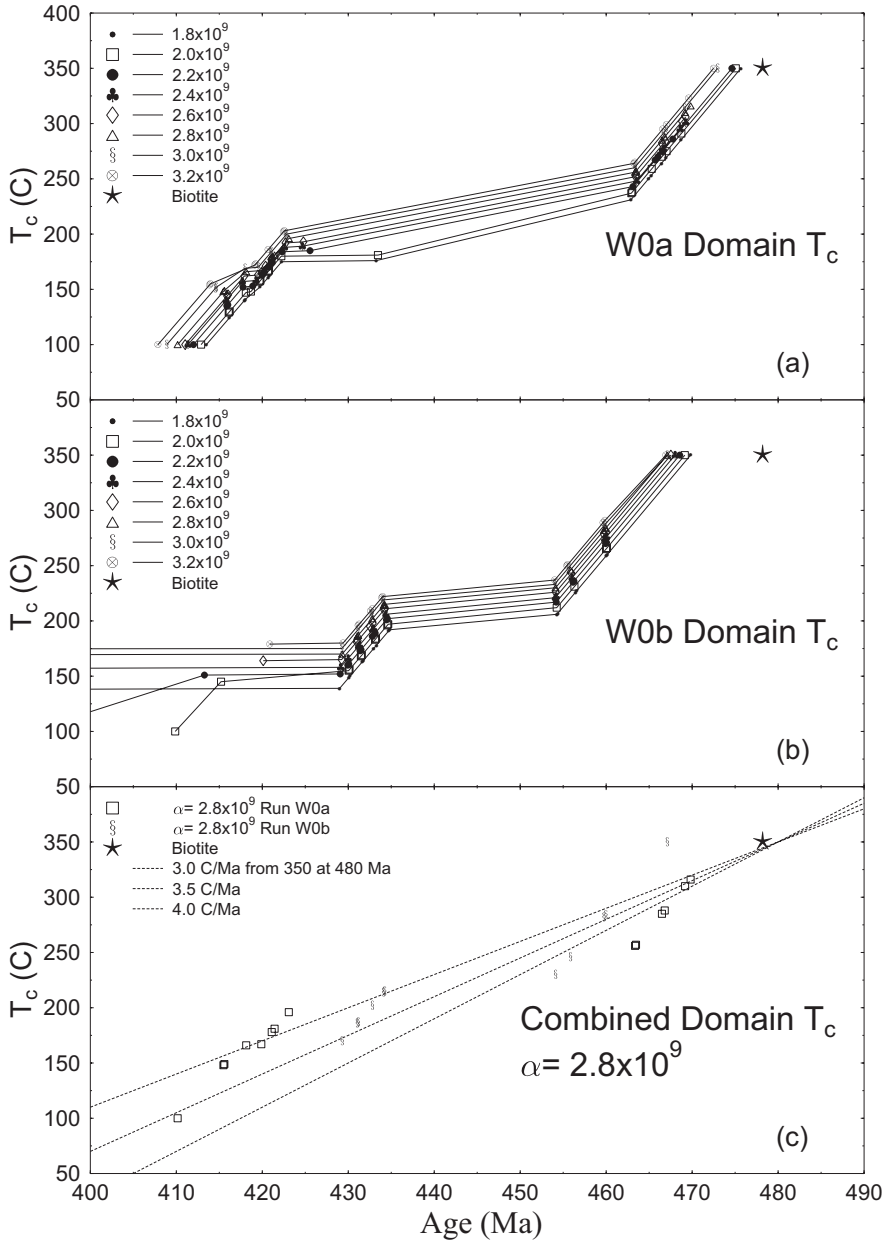
1.8x10^9
2.0x10^9
2.2x10^9
2.4x10^9
2.6x10^9
2.8x10^9
3.0x10^9
3.2x10^9
Biotite
W0a Domain Tc
(a)
W0b Domain Tc
(b)
α= 2.8x10^9 Run W0a
α= 2.8x10^9 Run W0b
3.0 C/Ma from 350 at 480 Ma
3.5 C/Ma
4.0 C/Ma
Combined Domain Tc
α= 2.8x10^9
(c)
Tc (C)
Age (Ma)

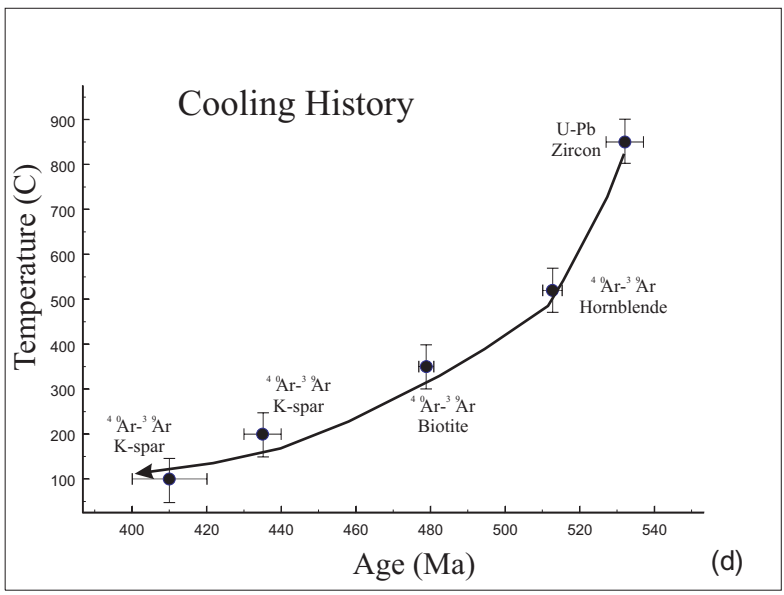
Cooling History
U-Pb Zircon
40Ar-39Ar Hornblende
40Ar-39Ar Biotite
40Ar-39Ar K-spar
40Ar-39Ar K-spar
Temperature (C)
Age (Ma)
(d)

Fig 5